Supplementary Materials: Transcription Factor RBPJL Is Able to Repress Notch Target Gene Expression but Is Non-Responsive to Notch Activation

Leiling Pan, Philipp Hoffmeister, Aleksandra Turkiewicz, N. N. Duyen Huynh, Andreas Große-Berkenbusch, Uwe Knippschild, J. Christof M. Gebhardt, Bernd Baumann, Tilman Borggrefe and Franz Oswald

Supplementary Figures:

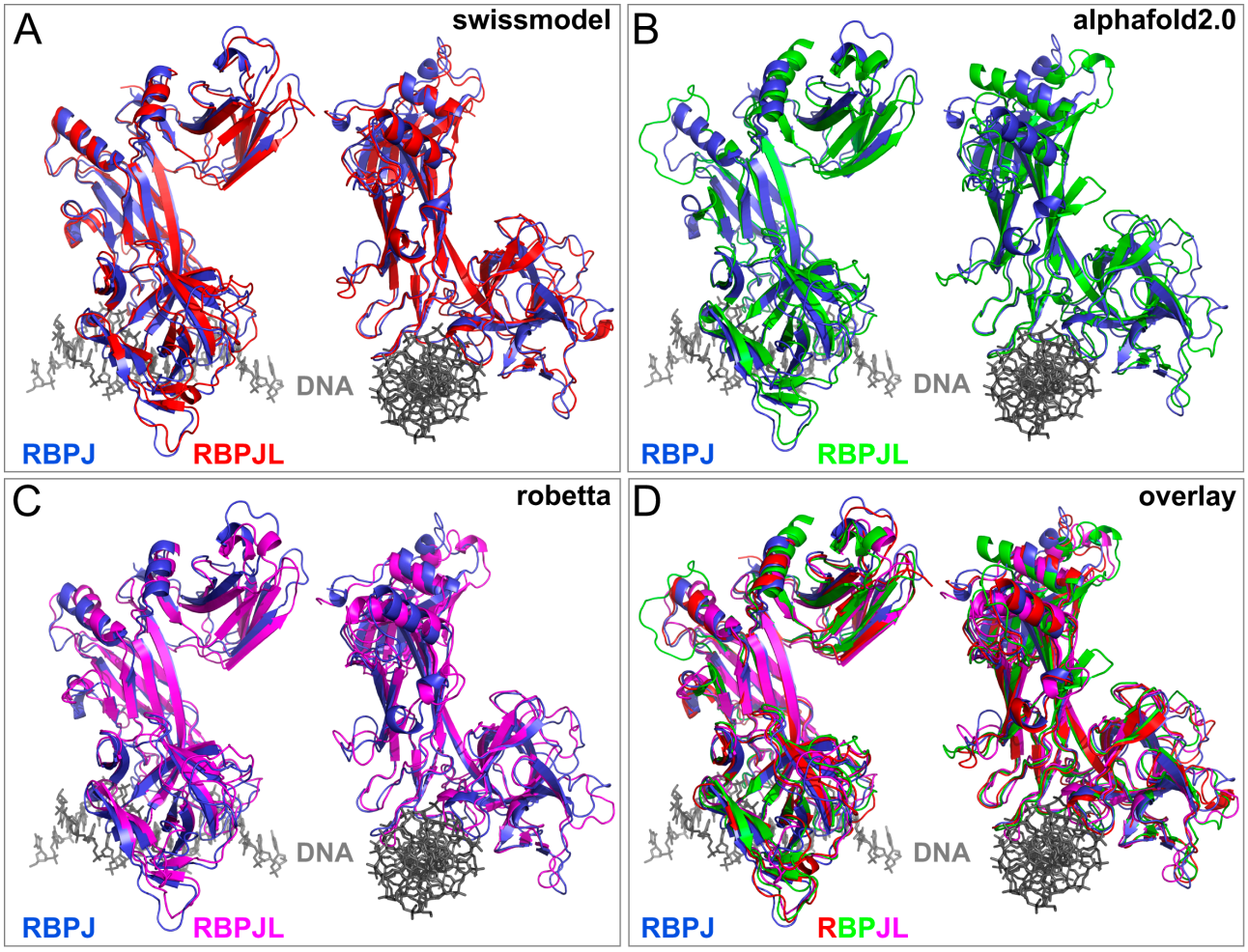

Figure S1. Structure prediction of RBPJL and alignment with the RBPJ crystal structure. Human RBPJ in complex with DNA was aligned with human RBPJL based on (A) homology modeling by swissmodel, (B) alphafold2.0 model [1], (C) robetta model [2] and (D) overlay of all three RBPJL models aligned to RBPJ bound to DNA (PDB entry 5EG6). The NTD, BTD and CTD domains are clear visible with all three models. The DNA is colored in grey. Right panels show the complexes after 90° rotation around a vertical axis revealing the responsible DNA binding regions of RBPJ and RBPJL. All structures as well as the alignment were performed using PyMOL (https://www.pymol.org).

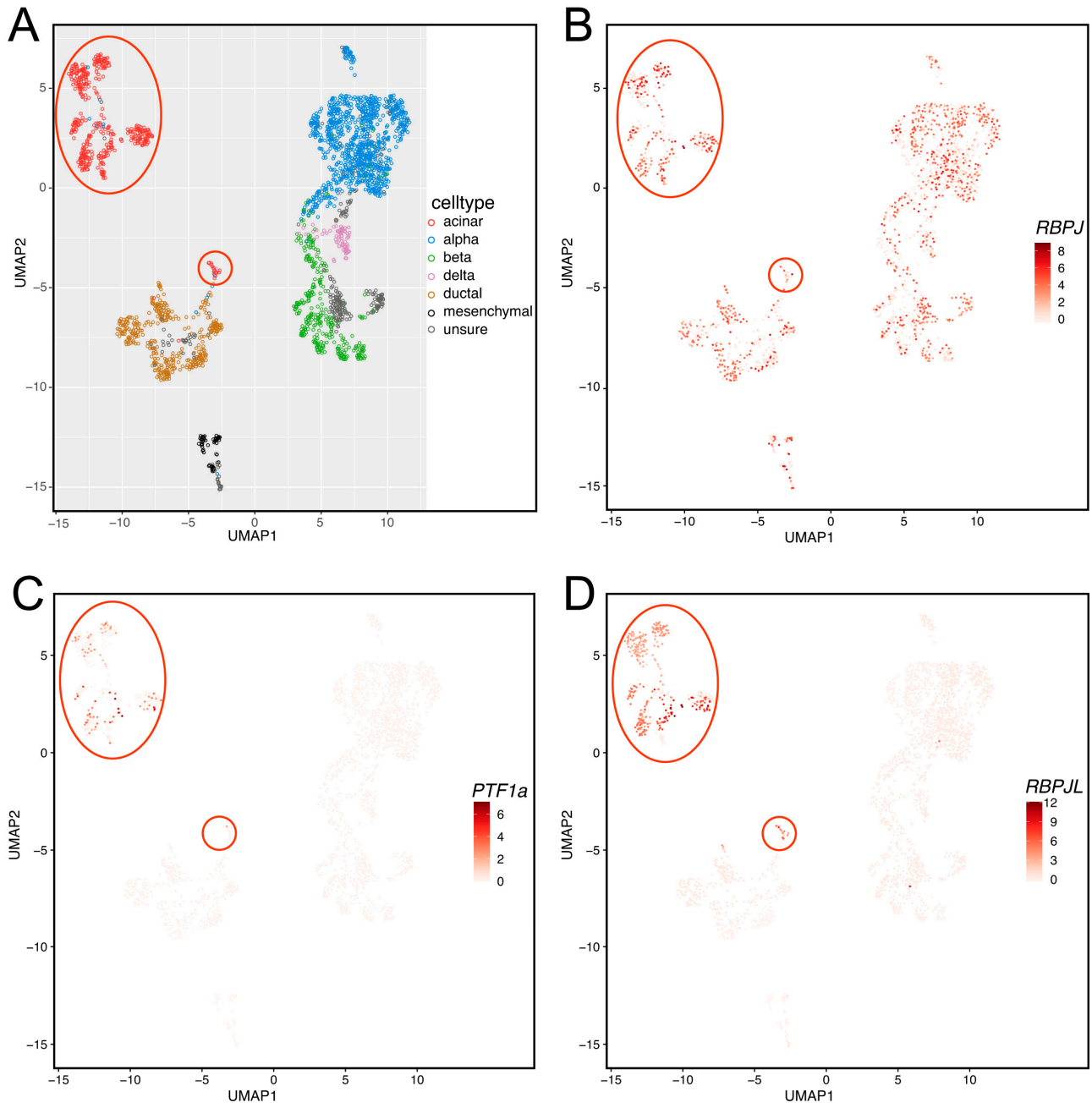

Figure S2. *RBPJL* is a highly acinar-specific marker (A) IUMAP projection of the cell types found in human adult pancreas established from single cell RNAseq. Each cluster of cells is defined by a specific color: acinar cells (red), alpha cells (blue), beta cells (green) delta cells (pink), ductal cells (brown), mesenchymal cells (black) and unsure (grey). Acinar cells are additionally highlighted by red circles. (B) IUMAP projection of *RBPJ* expression shows no cell type specificity in the adult human pancreas. (C and D) IUMAP projection of *PTF1a* (C) and *RBPJL* (D) show specific expression in the acinar compartment. The scRNAseq data set from human pancreas (GSE81547) [3] was reanalyzed as described in [4].

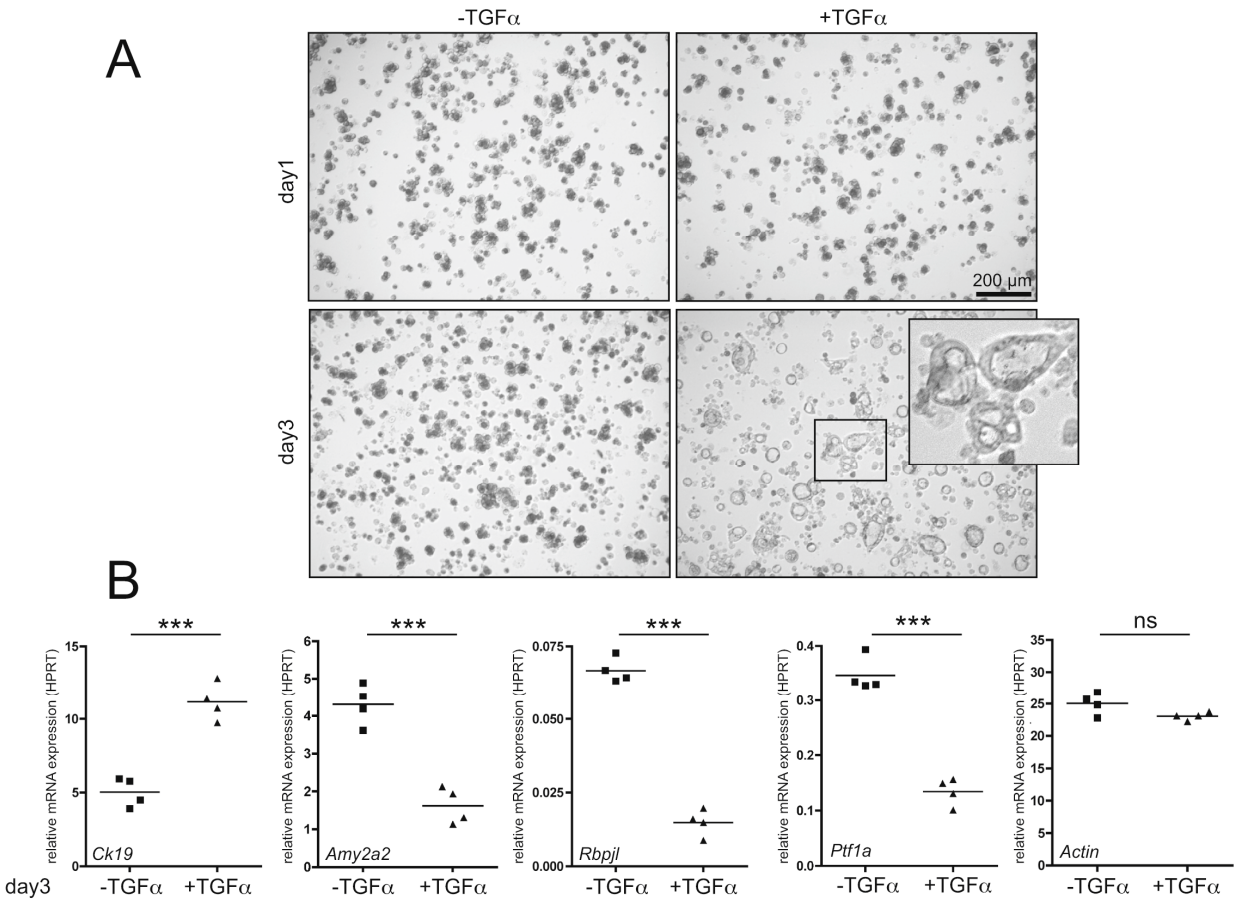

Figure S3. *Rbpjl* is downregulated during acinar to ductal differentiation *ex vivo:* (A) Primary acinar cells were isolated from 14-week old male mice (n=4) and cultivated in three-dimensional culture in growth factor reduced matrigel and transdifferentiation was induced by TGFα (500ng/well) as indicated. Pictures were taken 1 day and 3 days after seeding. Magnified region indicates ductal structures. Scale bar, 200 µm. (B) At day 3, mRNA was isolated from 3D cultures and relative mRNA expression of acinar markers (*Amy2a2, Ptfa*), ductal marker (*Ck19*), *Rbpjl*, and *Actin* were determined by qRT-PCR. All mRNA expressions studies are shown relative to *Hprt* expression. Mean values are from four independent experiments. *** indicates statistical significance ($p < 0.001$, ns = not significant, unpaired student's t-test).

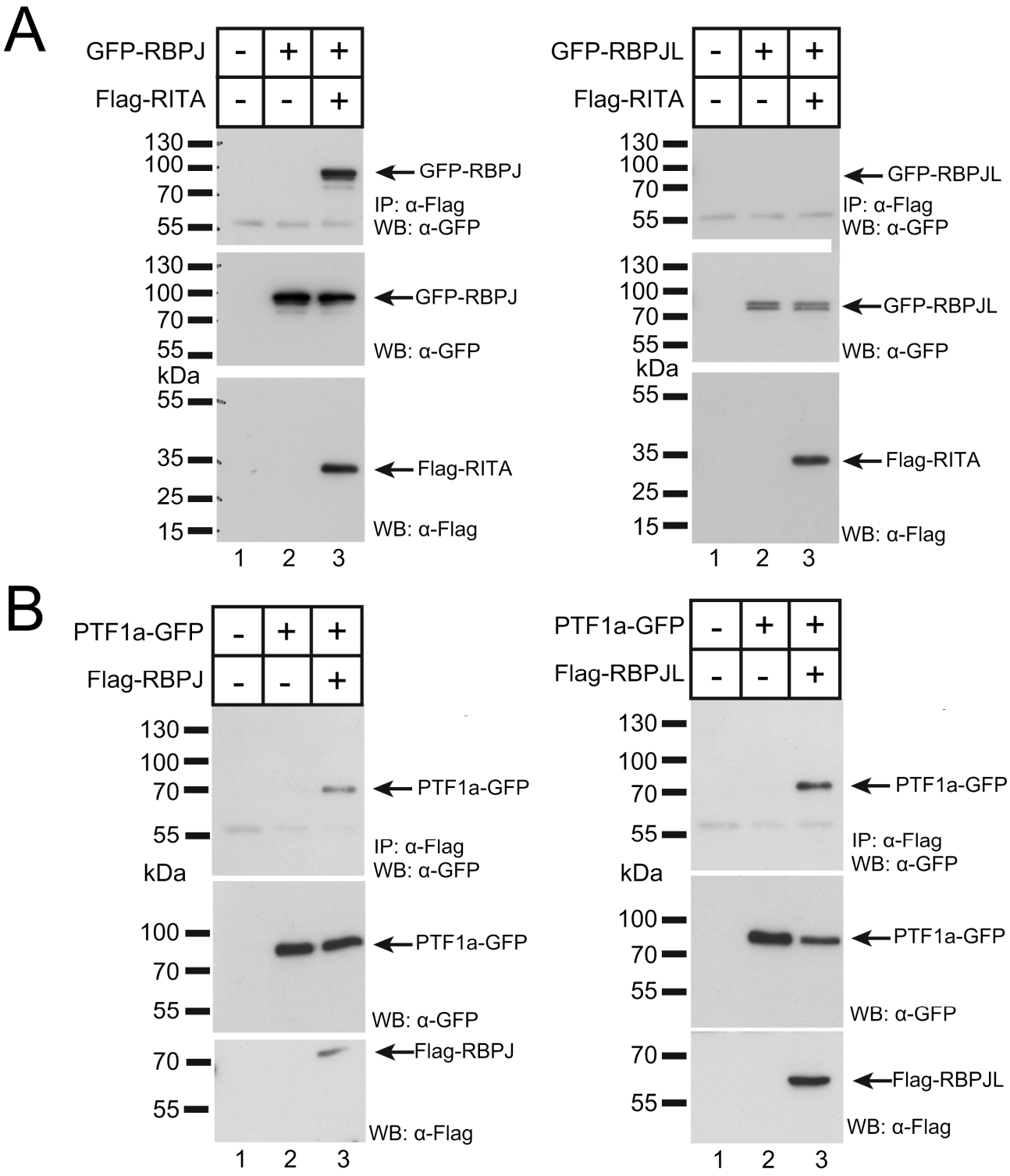

Figure S4. RBPJL does not interact with RBPJ-"RAM"-type binding protein RITA but interacts with PTF1a. (A) In contrast to RBPJ (left panel), coimmunoprecipitations (CoIPs) show no binding of RBPJL to RITA (A, right). HEK293 cells were cotransfected with GFP-tagged RBPJ or RBPJL together with Flag-tagged RITA. (B) RBPJ and RBPJL interact with PTF1a. HEK293 cells were cotransfected with Flag-tagged RBPJ or RBPJL together with GFP-tagged RITA. CoIPs were performed 24 h after transfection. Immunoprecipitation was performed using an anti-Flag antibody

and coimmunoprecipitated proteins were detected by using an anti-GFP antibody (upper panels). Expression of proteins was verified by Western blotting (middle panels and lower panels).

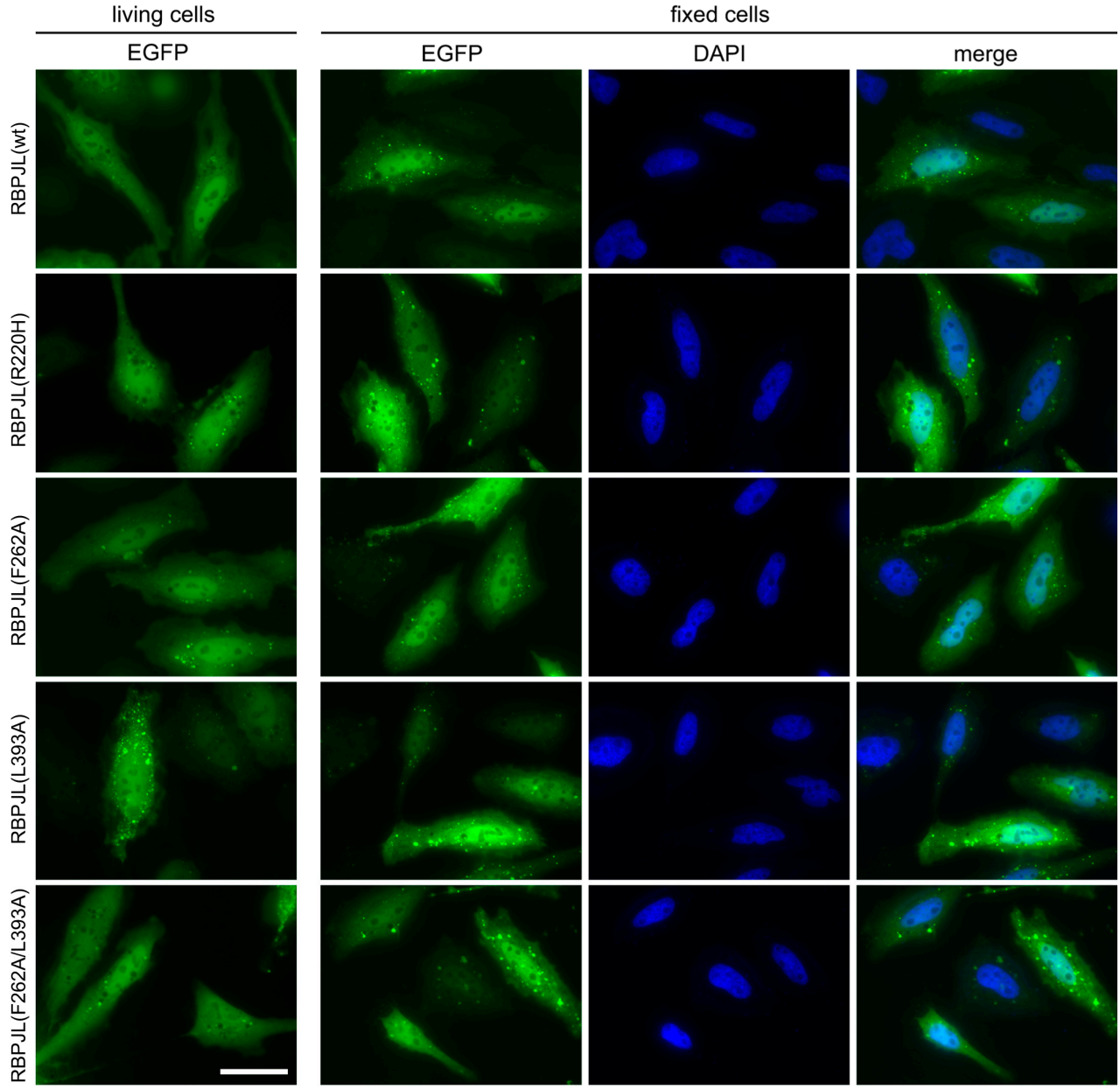

Figure S5. Subcellular localization of GFP-RBPJL variants. Subcellular localization of GFP-fused RBPJL (wt) and mutant proteins used in the study expressed in living cells (left row) and fixed cells (rows 2-4). HeLa cells were transfected with the indicated GFP-RBPJL constructs. 24 h after transfection, images of living cells were taken. Afterwards, cells were fixed and stained with DAPI. Images were taken using a fluorescence microscope equipped with a 63x lens. The superimposition of GFP with DAPI fluorescence in fixed cells (Row 4) shows that RBPJL is localized not only in the nucleus, but also in the cytoplasm. Scale bar, 20 μm.

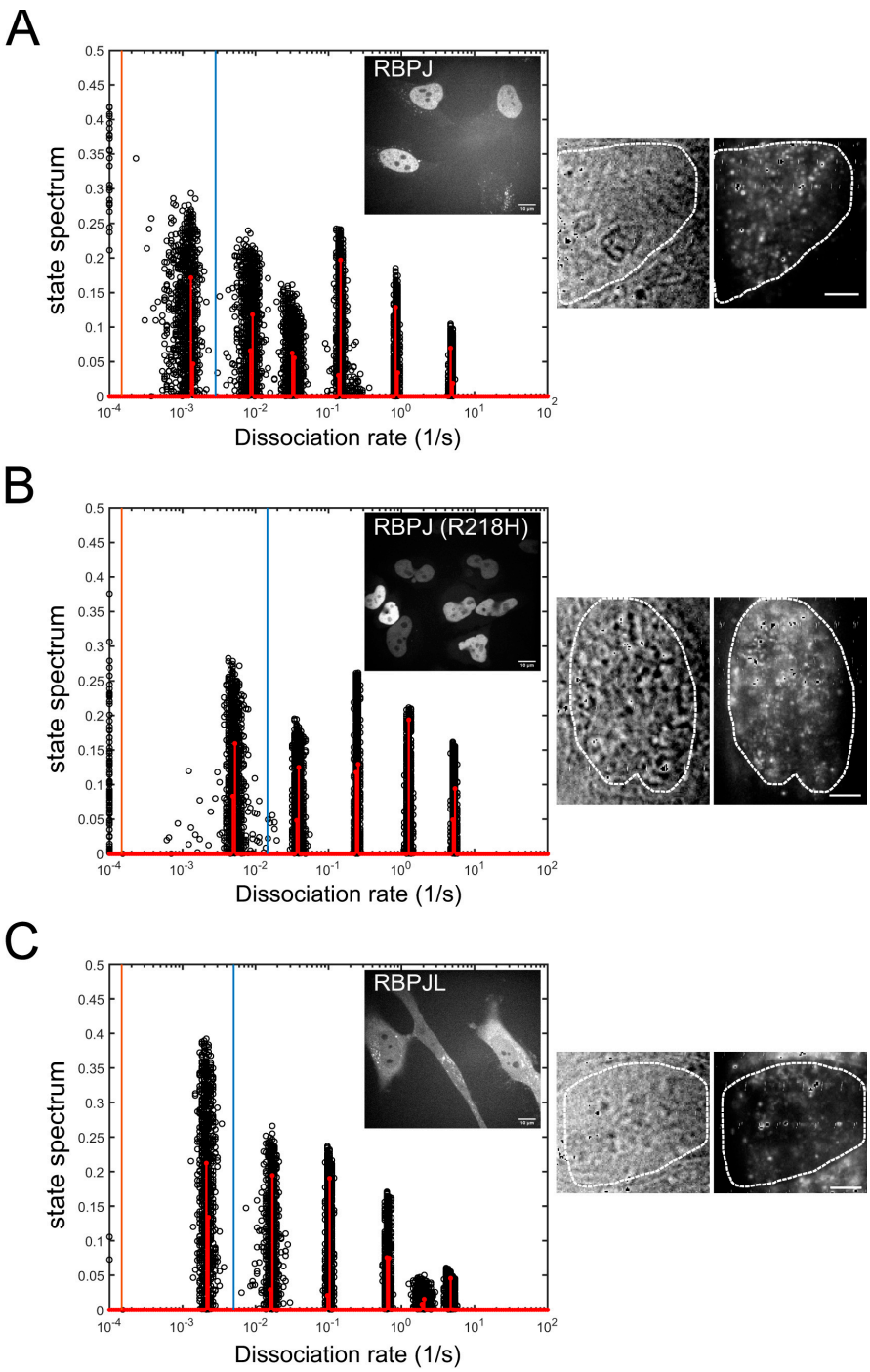

Figure S6. State spectra of RBPJ, RBPJ (R218H) and RBPJL. (A, B and C, left panels) State spectra of dissociation rates of RBPJ (A), RBPJ (R218H) (B) and RBPJL (C) obtained by GRID using all data (red bars) or by 499 GRID runs with random 80% of data as an error estimation of the state spectra (black circles). Residence time and standard deviation of the longest cluster were extracted by averaging data points (black circles) inside the borders set manually (orange and blue lines). Average dissociation rate (1/s) ± s.d. (1/s): RBPJ: 0.0011 ± 0.0003; RBPJ (R218H): 0.0052 ± 0.0007; RBPJL: 0.0022 ± 0.0003. Scale bar, 10 μm. Right panels: Representative bright field images of cells expressing Halo-tagged RBPJ, RBPJ (R218H) and RBPJL and standard deviation of all frames of a single-molecule movie. White dotted line depicts the outline of the nucleus. Scale bar, 4 μm.

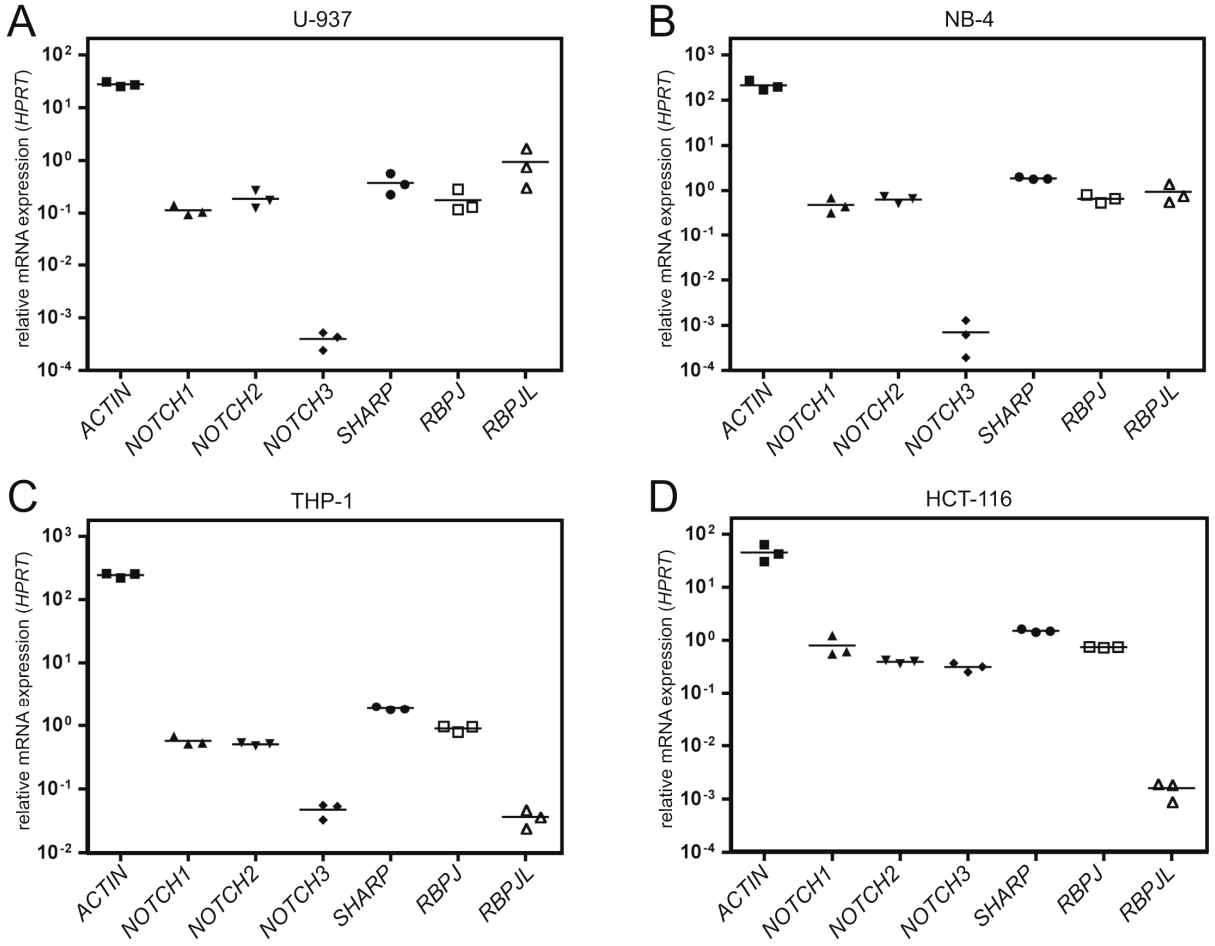

Figure S7. Expression of RBPJL in non-pancreatic tumour cells: mRNA expression of *ACTIN*, Notch pathway components *NOTCH1*, *NOTCH2*, *NOTCH3*, *SHARP*, *RBPJ* and *RBPJL* in the cell lines (A) U-937 (histiocytic lymphoma), (B) NB-4 (acute promyelocytic leukemia), (C) THP-1 (acute monocytic leukemia) and (D) HCT-116 (colorectal carcinoma). In the cell lines U-937 and NB-4 *RBPJL* expression is similar or even higher than the expression of *RBPJ*. The mRNA expression levels are represented relative to the housekeeping gene *HPRT* from three independent experiments.

to Figure 3A

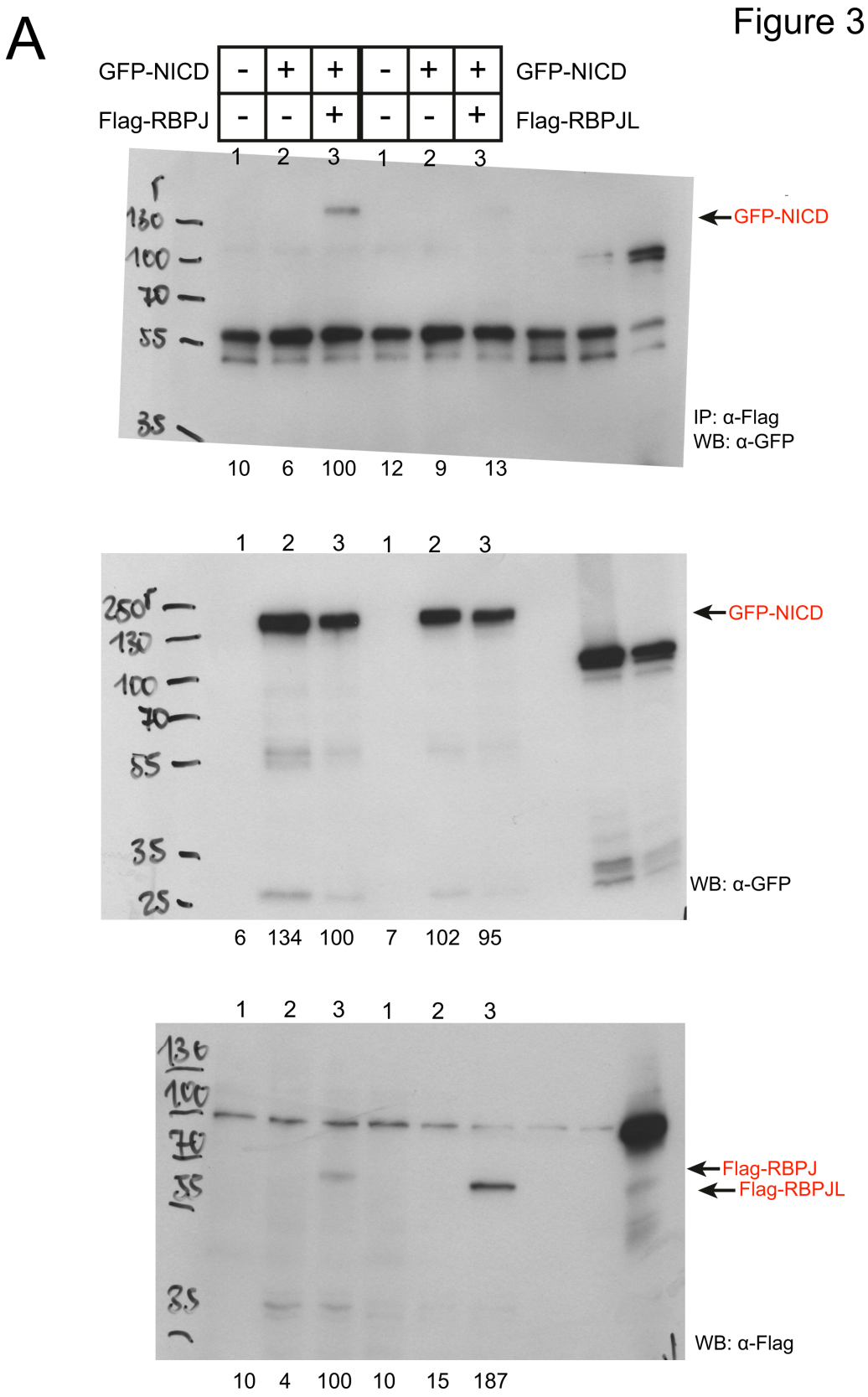
A
Figure 3
GFP-NICD - + + - + + GFP-NICD
Flag-RBPJ - - + - - + Flag-RBPJL
1 2 3 1 2 3
130
100
70
55
35
GFP-NICD
IP: α-Flag
WB: α-GFP
10 6 100 12 9 13
1 2 3 1 2 3
250
130
100
70
55
35
25
GFP-NICD
WB: α-GFP
6 134 100 7 102 95
1 2 3 1 2 3
130
100
70
55
35
Flag-RBPJ
Flag-RBPJL
WB: α-Flag
10 4 100 10 15 187

to Figure 3B

Figure 3

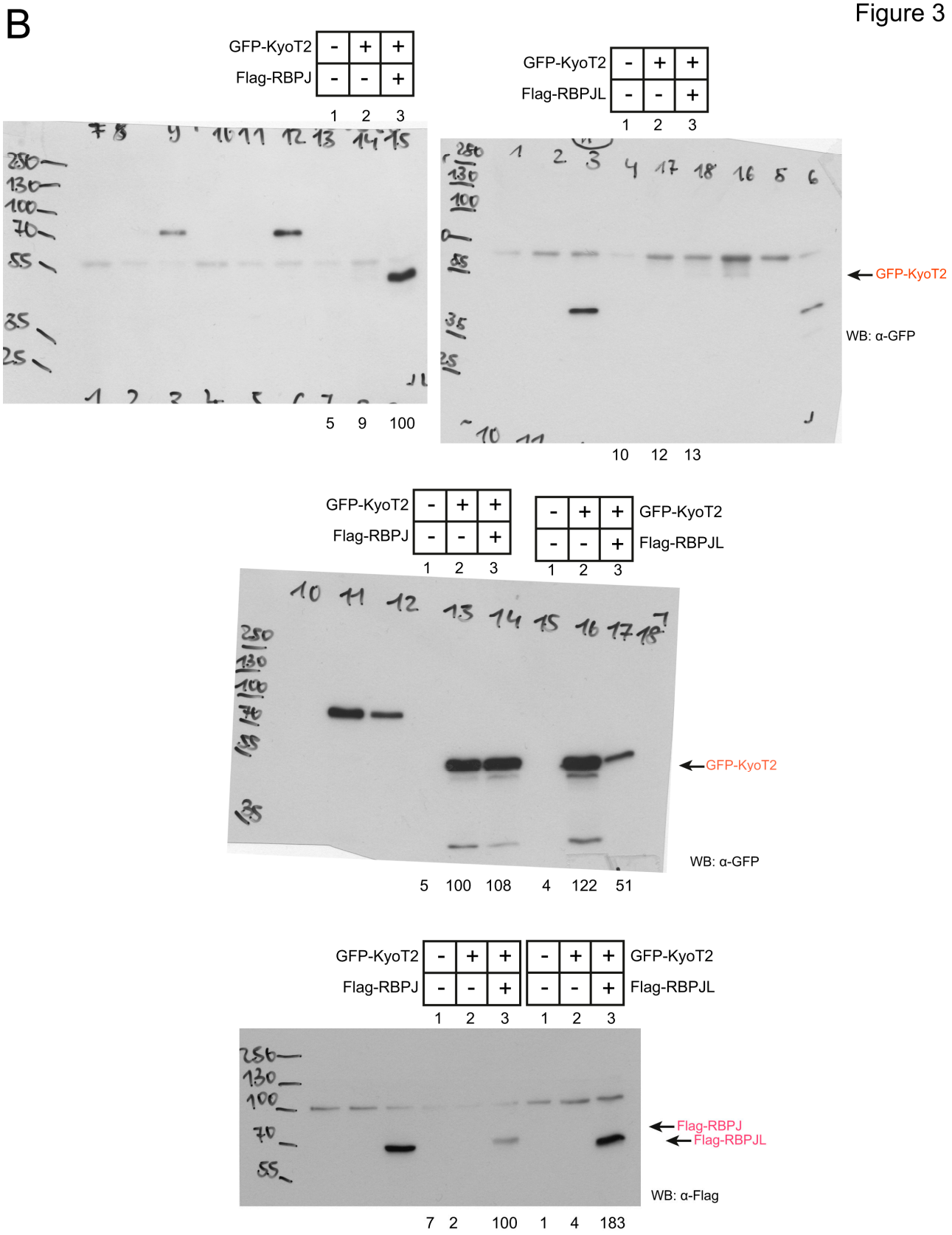

to Figure 3C

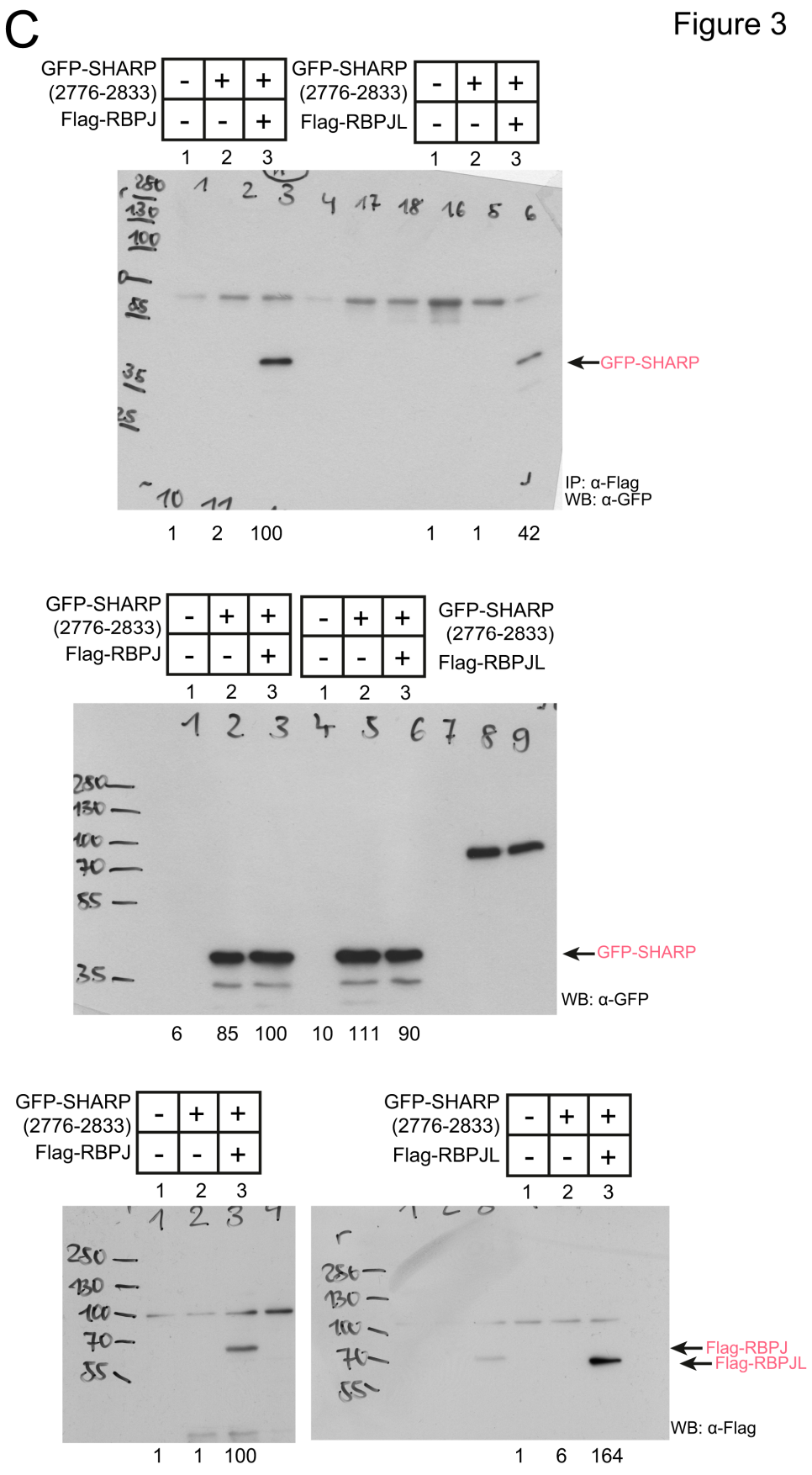
C
Figure 3
GFP-SHARP (2776-2833)
Flag-RBPJ
Flag-RBPJL
GFP-SHARP
IP: α-Flag
WB: α-GFP
WB: α-Flag
Flag-RBPJ
Flag-RBPJL

to Figure 4B

B

Figure 4

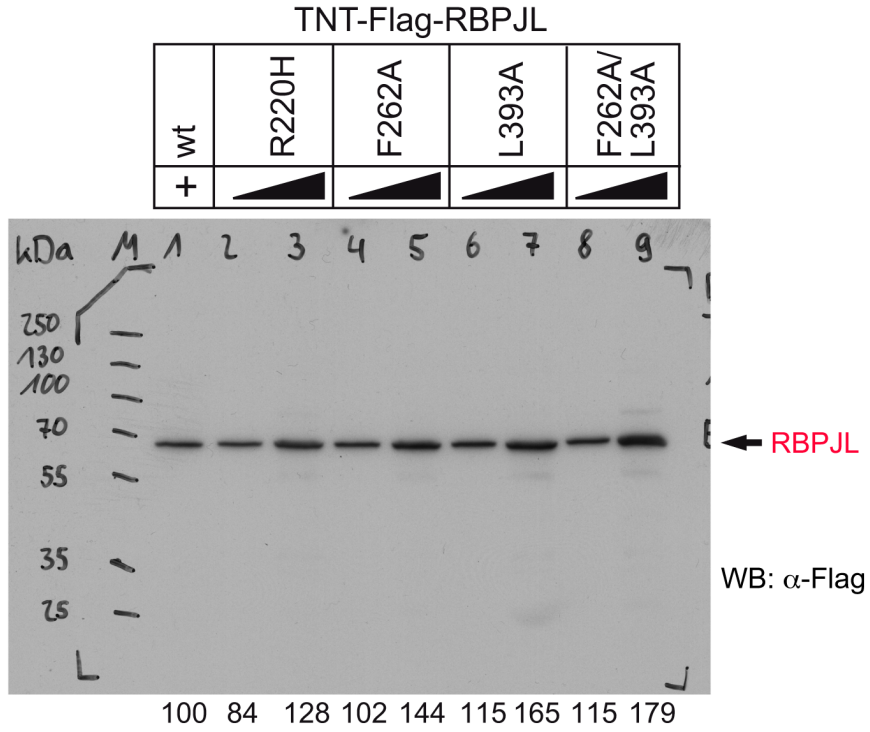

to Figure 6D

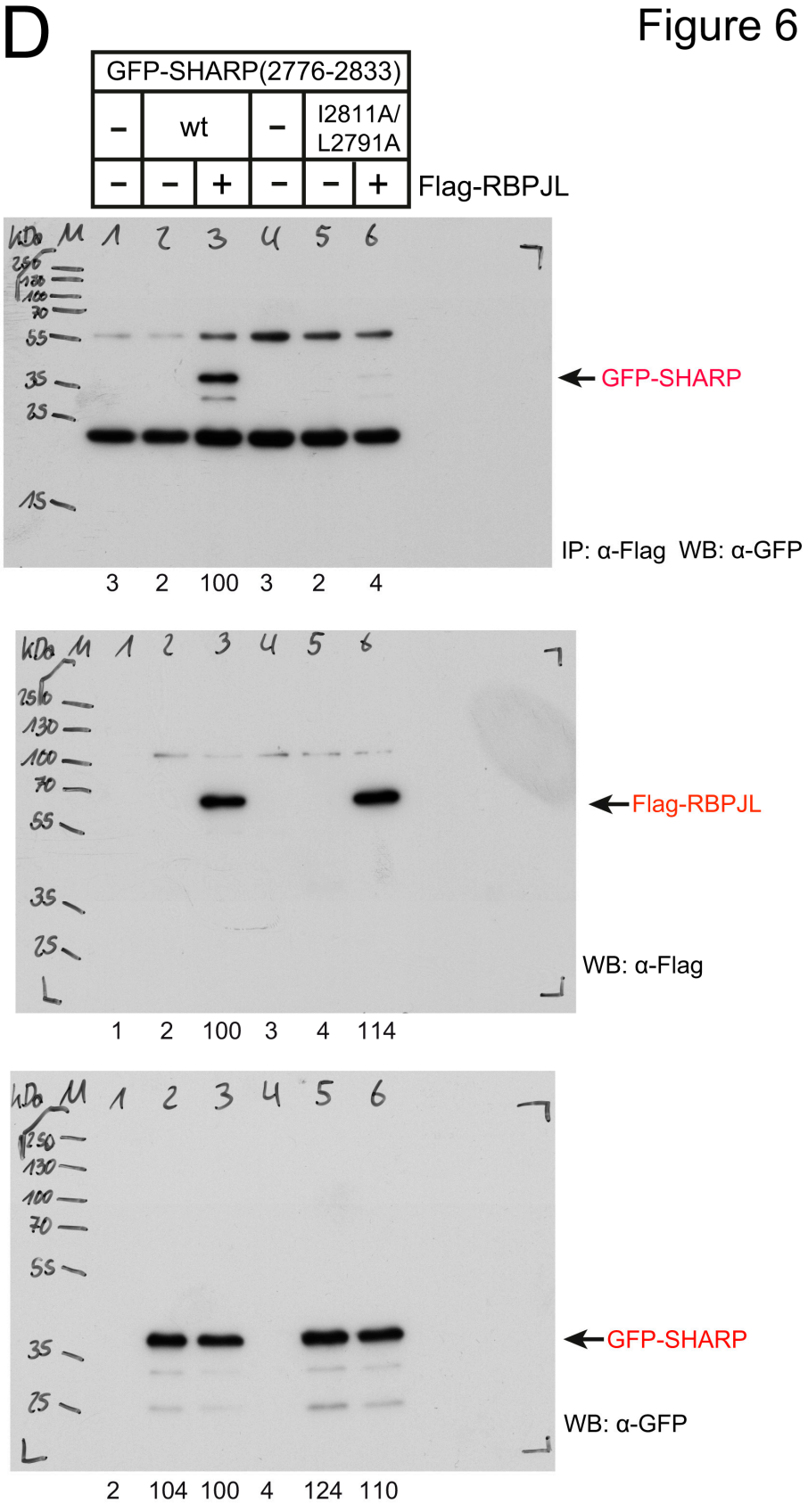
D
Figure 6
GFP-SHARP(2776-2833)
–
wt
–
I2811A/
L2791A
– – + – – +
Flag-RBPJL
kDa M 1 2 3 4 5 6
250
130
100
70
55
35
25
15
GFP-SHARP
IP: α-Flag WB: α-GFP
3 2 100 3 2 4
kDa M 1 2 3 4 5 6
250
130
100
70
55
35
25
Flag-RBPJL
WB: α-Flag
1 2 100 3 4 114
kDa M 1 2 3 4 5 6
250
130
100
70
55
35
25
GFP-SHARP
WB: α-GFP
2 104 100 4 124 110

to Figure 6E

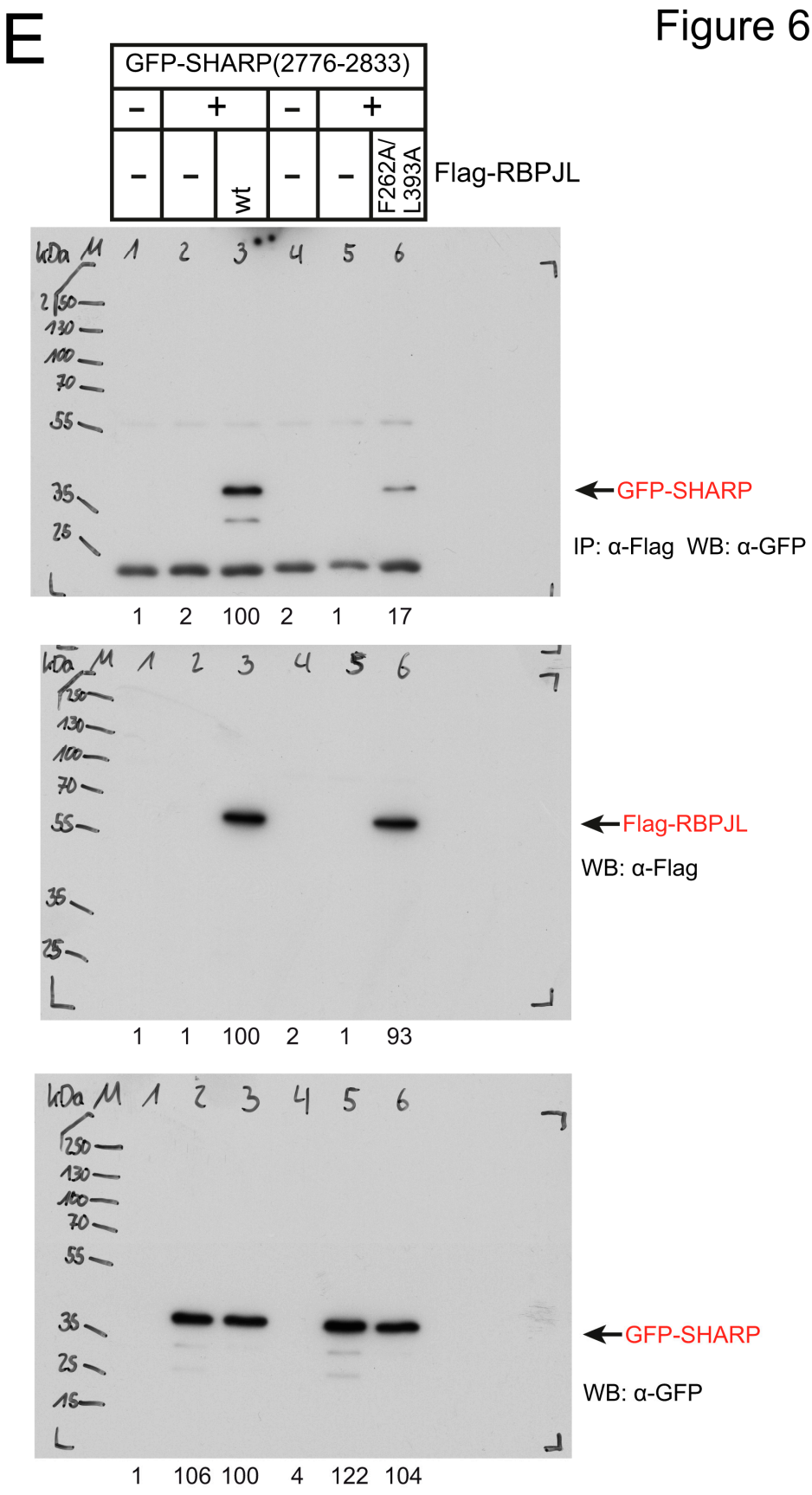
E
Figure 6
GFP-SHARP(2776-2833)
-
+
-
+
-
-
wt
-
-
F262A/
L393A
Flag-RBPJL
kDa M 1 2 3 4 5 6
250
130
100
70
55
35
25
GFP-SHARP
IP: α-Flag WB: α-GFP
1 2 100 2 1 17
kDa M 1 2 3 4 5 6
250
130
100
70
55
35
25
Flag-RBPJL
WB: α-Flag
1 1 100 2 1 93
kDa M 1 2 3 4 5 6
250
130
100
70
55
35
25
15
GFP-SHARP
WB: α-GFP
1 106 100 4 122 104

to Figure 7

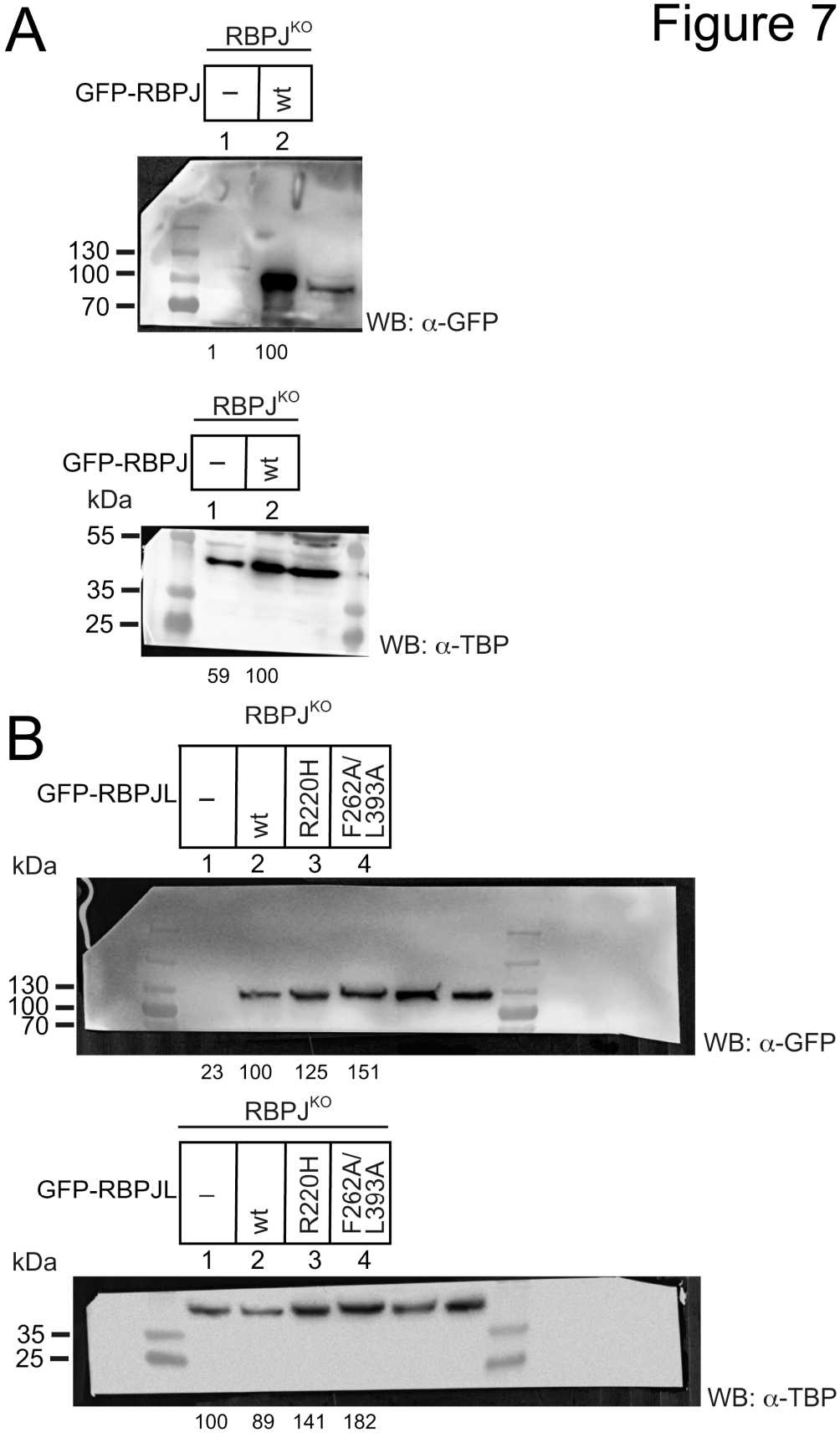
Figure 7
A
RBPJKO
GFP-RBPJ
–
wt
1 2
130
100
70
WB: α-GFP
1 100
RBPJKO
GFP-RBPJ
–
wt
kDa
1 2
55
35
25
WB: α-TBP
59 100
B
RBPJKO
GFP-RBPJL
–
wt
R220H
F262A/
L393A
kDa
1 2 3 4
130
100
70
WB: α-GFP
23 100 125 151
RBPJKO
GFP-RBPJL
–
wt
R220H
F262A/
L393A
kDa
1 2 3 4
35
25
WB: α-TBP
100 89 141 182

to Figure S4A

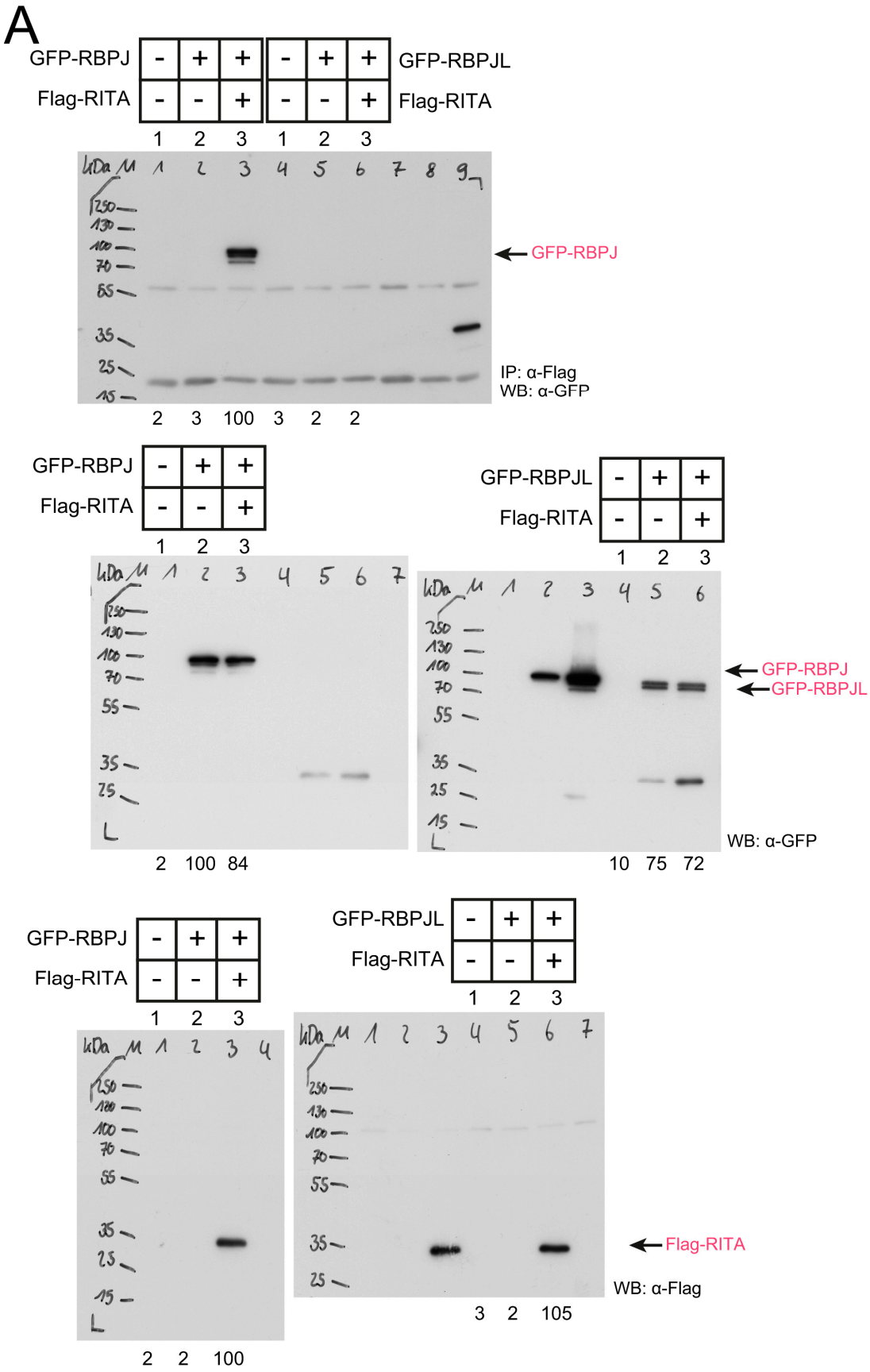

to Figure S4B

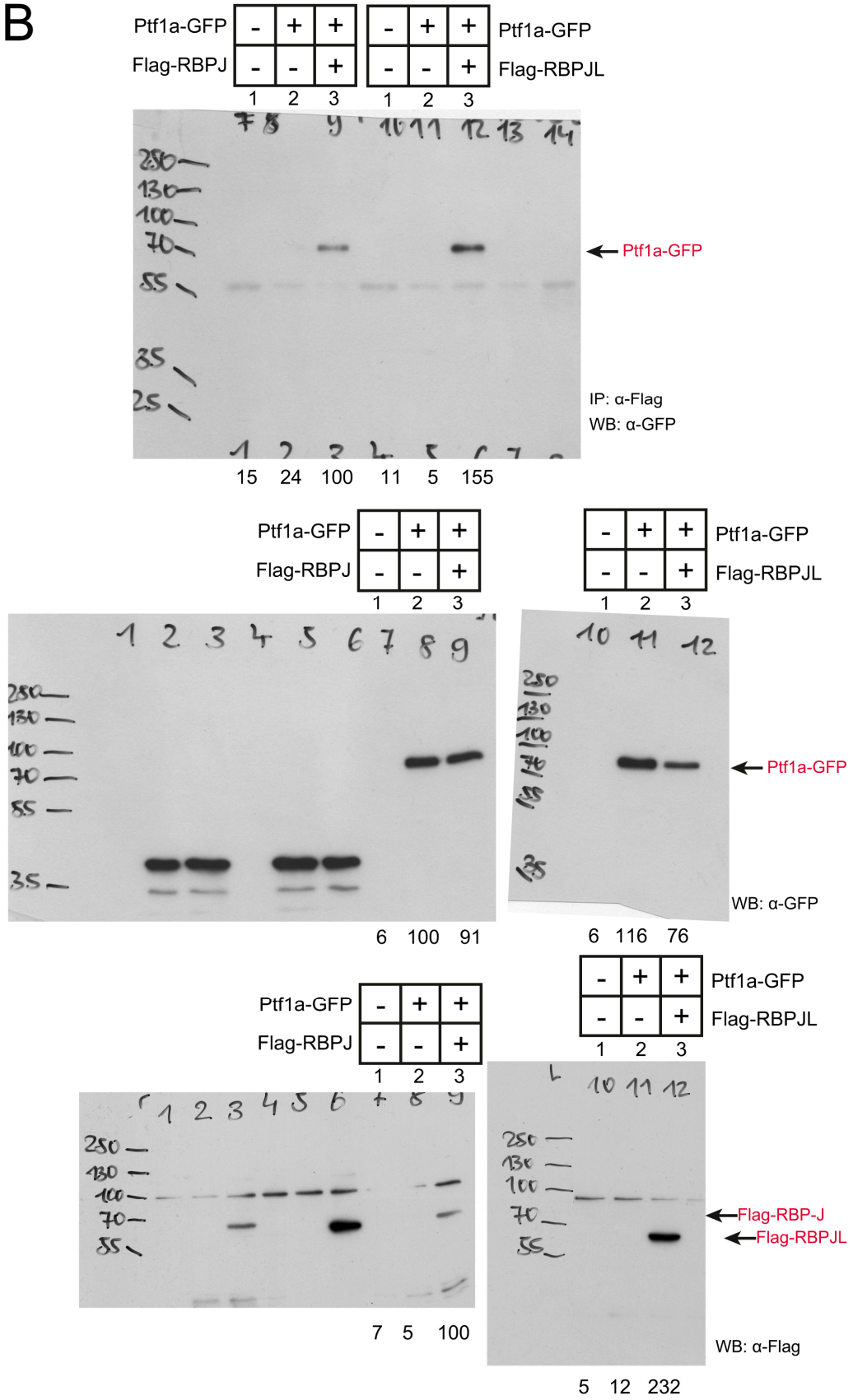

Figure S8. Whole western blots including size markers and relative densitometric values of relevant bands.

References

1. Jumper, J.; Evans, R.; Pritzel, A.; Green, T.; Figurnov, M.; Ronneberger, O.; Tunyasuvunakool, K.; Bates, R.; Zidek, A.; Potapenko, A.; et al. Highly accurate protein structure prediction with AlphaFold. *Nature* **2021**, *596*, 583–589, doi:10.1038/s41586-021-03819-2.
2. Baek, M.; DiMaio, F.; Anishchenko, I.; Dauparas, J.; Ovchinnikov, S.; Lee, G.R.; Wang, J.; Cong, Q.; Kinch, L.N.; Schaeffer, R.D.; et al. Accurate prediction of protein structures and interactions using a three-track neural network. *Science* **2021**, *373*, 871–876, doi:10.1126/science.abj8754.
3. Enge, M.; Arda, H.E.; Mignardi, M.; Beausang, J.; Bottino, R.; Kim, S.K.; Quake, S.R. Single-Cell Analysis of Human Pancreas Reveals Transcriptional Signatures of Aging and Somatic Mutation Patterns. *Cell* **2017**, *171*, 321–330 e314, doi:10.1016/j.cell.2017.09.004.
4. Breunig, M.; Merkle, J.; Wagner, M.; Melzer, M.K.; Barth, T.F.E.; Engleitner, T.; Krumm, J.; Wiedenmann, S.; Cohrs, C.M.; Perkhofer, L.; et al. Modeling plasticity and dysplasia of pancreatic ductal organoids derived from human pluripotent stem cells. *Cell Stem Cell* **2021**, *28*, 1105–1124 e1119, doi:10.1016/j.stem.2021.03.005.